Institute of Paper Science and Technology
Atlanta, Georgia

IPST Technical Paper Series Number 717

Flotation Deinking Fluid Mechanics Research at IPST

T.J. Heindel

April 1998

Submitted to
Paper Recycling Challenges, Vol. III—Process Technology

INSTITUTE OF PAPER SCIENCE AND TECHNOLOGY
PURPOSE AND MISSIONS

The Institute of Paper Science and Technology is a unique organization whose charitable, educational, and scientific purpose evolves from the singular relationship between the Institute and the pulp and paper industry which has existed since 1929. The purpose of the Institute is fulfilled through three missions, which are:

- to provide high quality students with a multidisciplinary graduate educational experience which is of the highest standard of excellence recognized by the national academic community and which enables them to perform to their maximum potential in a society with a technological base; and
- to sustain an international position of leadership in dynamic scientific research which is participated in by both students and faculty and which is focused on areas of significance to the pulp and paper industry; and
- to contribute to the economic and technical well-being of the nation through innovative educational, informational, and technical services.

ACCREDITATION

The Institute of Paper Science and Technology is accredited by the Commission on Colleges of the Southern Association of Colleges and Schools to award the Master of Science and Doctor of Philosophy degrees.

NOTICE AND DISCLAIMER

The Institute of Paper Science and Technology (IPST) has provided a high standard of professional service and has put forth its best efforts within the time and funds available for this project. The information and conclusions are advisory and are intended only for internal use by any company who may receive this report. Each company must decide for itself the best approach to solving any problems it may have and how, or whether, this reported information should be considered in its approach.

IPST does not recommend particular products, procedures, materials, or service. These are included only in the interest of completeness within a laboratory context and budgetary constraint. Actual products, procedures, materials, and services used may differ and are peculiar to the operations of each company.

In no event shall IPST or its employees and agents have any obligation or liability for damages including, but not limited to, consequential damages arising out of or in connection with any company's use of or inability to use the reported information. IPST provides no warranty or guaranty of results.

FLOTATION DEINKING FLUID MECHANICS RESEARCH AT IPST

Theodore J. Heindel
Assistant Professor of Engineering
Institute of Paper Science and Technology
500 10th Street NW
Atlanta, GA 30318-5794

ABSTRACT

Fluid mechanic issues related to effective contaminant removal by flotation are being addressed at the Institute of Paper Science and Technology. This review summarizes that research. A method to visualize gas flows in fiber suspensions is first reviewed and flow visualization results are shown. Gas holdup measurements in a fiber suspension are then discussed and selected results are outlined. Mixing studies in pulp suspensions are also detailed. Finally, flotation modeling efforts are briefly reviewed.

KEYWORDS

fluid mechanics, flotation, deinking, fluid flow, flash x-ray radiography, gamma densitometry, mixing, wax

1. INTRODUCTION

Paper recycling is a complex issue where the main goal is to remove as many contaminants as possible while retaining as many fibers as possible. This is typically accomplished through a variety of separation processes, including screening, cleaning, flotation, and washing. In all of these processes, the understanding of the relevant fluid mechanic issues is critical for effective contaminant removal. This article reviews the current research program at the Institute of Paper Science and Technology (IPST) in the area of flotation deinking fluid mechanics, which has been ongoing for approximately four years. This program examines air bubble flow visualization and bubble size measurements in pulp suspensions at consistencies typical of flotation deinking, gas holdup measurements in a bubble column under various operating conditions, mixing in a fiber suspension and its relationship to contaminant size, and bubble/particle interactions and the development of a flotation deinking model. Stickies interactions and control [1] and flotation deinking chemistry [2] are also being addressed at IPST but will not be included in this review.

2. BUBBLE VISUALIZATION

A greater understanding of the bubble flow characteristics and the bubble size in an air/water/fiber suspension is important to many paper processing areas such as flotation deinking and bleaching with gaseous chemicals. These parameters can easily be measured in a transparent (i.e., gas/water) system by optical visualization and/or laser techniques [3-7]. If the system is opaque, optical and laser techniques can only be utilized near the system boundaries, if at all. However, the walls encompassing the system can influence the information obtained and this information may not represent true conditions in the bulk flow. For these systems, resistivity or optical probes have been suggested, but they would be inadequate in a fiber suspension because the fiber could form entanglements around the probe tip. Therefore, alternative tools and techniques must be developed to characterize the bubble behavior in complex gas/liquid/fiber systems, such as flotation deinking cells.

Attempts to visualize these complex fiber suspensions have been conducted by Walmsley [8] where water was replaced by clove oil to produce a system that had the same refractive index as wood fiber. However, the applicability of these results to air/water/fiber systems is unknown. Additional experiments have been performed to measure bubble size in dilute fiber systems of less than 0.5% consistency by weight by Hunold et al. [9]. Small samples were siphoned through a capillary tube from the experimental test cell and analyzed for bubble volume. The effective bubble diameter was then determined. Possible bubble coalescence in the siphoning procedure or capillary tube were not addressed in this study. Julien Saint Amand [10] has also addressed the effect of bubble size on flotation, but bubble size was measured in a fiber-free system and assumed to not change when fiber was added to the flotation cell. We are developing alternative techniques to quantify flow characteristics and bubble size in fiber suspensions.

2.1 Flash X-ray Radiography

Radiation techniques offer the ability to penetrate opaque fiber systems without inserting flow-altering probes. Flash x-ray radiography (FXR) is an x-ray imaging process where an intense burst of radiation is produced for a fraction of a second to record dynamic events on film that may be obscured by dust, smoke, or light, conditions that would make conventional high-speed photography impossible. FXR also allows for the recording of images of inclusions or voids inside opaque objects that are part of these dynamic events.

The application of FXR to air/water/fiber flows is justified because water and wood fibers have similar densities, whereas the density of air is considerably different from water and wood fiber. Water also has a linear x-ray attenuation coefficient (a measure of x-ray absorption) three orders of magnitude larger than air, and a suspension of wood fiber and water should absorb x-rays in a similar manner, unless the water or fiber has been treated with special radioactive materials. Hence, water and wood fibers will absorb x-rays at a similar rate, but at a significantly different rate compared to air.

FXR has been used periodically over the past 10 years at IPST to study areas relevant to the pulp and paper industry. Farrington used FXR to study high consistency forming [11] and demonstrated that FXR is a potentially powerful technique for the investigation of high-speed multiphase flows in general and concentrated fiber flows in particular. He extended this technique to investigate sheet formation and quality [12] and black liquor spray formation [13]. Triantafillopoulos and Farrington [14] further extended this technique to visualize flow phenomena in opaque coating applications. Finally, Zavaglia and Lindsay [15] applied FXR and an x-ray tracing fluid to visualize fluid motion during impulse drying. These processes are similar in that the events of interest typically occur at high speed and the region of visual interest is obscured – a condition that is ideal for FXR application.

We recently utilized FXR to visualize air flows in a suspension of unprinted old newspaper (ONP) at various consistencies and air flow rates [16-18]. This was accomplished in a quiescent rectangular bubble column (no bulk fluid exchange) depicted in Fig. 1, which had interior dimensions of 20 cm wide by 2 cm deep, and was 100 cm high. Air was injected at the base of the column through nine evenly spaced holes. A single 20 cm × 25.2 cm x-ray negative was exposed during the 30 nanosecond discharge of the x-ray unit, freezing the image on film. Composite images were formed at three column locations to gather qualitative results of the gas flow conditions.

2.2 Bubble Flow Observations

Figure 2 displays composite radiographs obtained in an air/water system at three different air injection rates, where the arrows at the base of each column represent the relative locations of each air inlet hole. The x-rays of each column represent the composite of individual x-rays taken at one of three positions in the quiescent bubble column and at separate time intervals. Position 1 and Position 3 correspond to the bottom and top image, respectively. The gaps, or open areas between each x-ray position are due to film placement restrictions on the bubble column. The actual image area of the column interior is 20 cm × 20 cm. The radiographs, as shown in the format presented here, have some loss of detail as a result of electronic digitization and reduction, but the images are representative of the originals, which are available at IPST. All observations and measurements in our studies are based on the original images.

Figure 2a corresponds to an air injection flow rate of 0.5 slpm (standard liters per minute) and shows discrete air bubbles (the dark regions) rising through the water column in a well-dispersed fashion. This flow pattern is typically referred to as bubbly flow [19]. Upon close examination of each radiograph, the bubbles appear to be ellipsoidal in shape with a major axis length between approximately 2 and 5 mm, indicating the bubbles are fairly uniform in size compared to other test conditions (i.e., Fig. 2c). The observed bubbles are not spherical because drag forces tend to deform the bubble shape. Although the bubbles may differ considerably from true ellipsoids, they are commonly classified as ellipsoidal [3]. The air/water flow patterns observed at 0.5 slpm continue throughout the column height, with negligible evidence of bubble coalescence. These observations are also confirmed by visual examination of the air/water flow characteristics before and after the radiographs were taken.

Increasing the air injection flow rate to 2.0 slpm (Fig. 2b) results in the appearance of many more bubbles. Some of the bubbles appear to be clumped together in groups, and it is hypothesized that these bubble groups will coalesce to form a single larger bubble if the thin liquid film between the bubbles has sufficient time to thin and rupture before the bubbles break the surface. Additionally, some larger bubbles are also observed which are more than likely formed by the coalescence of these groups of smaller bubbles. Coalescence is further verified by the observations of more larger bubbles being recorded at Position 3 than at Position 1. Hence, they coalesce as they rise through the column. The flow regime associated with this air injection rate is still considered bubbly, or beginning the transition from bubbly flow, because the flow remains predominantly homogeneous.

At an air injection flow rate of 15 slpm (Fig. 2c), the flow is now considered to be churn-turbulent [19], characterized by a heterogeneous flow of rather large bubbles that form by the coalescence of smaller bubbles, with some smaller bubbles still present throughout the column. The large dark regions in these radiographs correspond to single large bubbles. Some

are formed at the column base as the air is introduced into the column at these high air injection rates. Others form as the bubbles rise through the column and interact with each other in this highly turbulent flow. At these high air injection rates, backmixing is visually observed in the column, where large bubbles (that may span the 2 cm column depth) travel up the central region of the column in a serpentine pattern and smaller bubbles adjacent to the walls travel downward, trapped in the backmixed flow around the oscillating rising channels of air. The smaller bubbles are eventually caught in the rising bulk flow. Backmixing is not captured on the radiographs nor is it recorded on photographs; however, it is possible to record this phenomenon by high-speed video analysis if the system is transparent.

Adding 1% unprinted ONP to the system results in a significant change in the bubble flow characteristics. At an air injection flow rate of 0.5 slpm (Fig. 3a), there are preferential regions at the base of the column (Position 1) where the air bubbles rise and other regions are void of rising bubbles. This is a result of fiber network formation that restricts the rise of small bubbles. When a bubble is large enough to break through the fiber network, or a bubble finds a local region where no network exists, the bubbles rise. As they rise, they push the fiber aside creating local regions with a fiber consistency less than the average value of 1% and other regions where the local consistency is greater than 1%. The locally low consistency regions have a low resistance to bubble rise, creating the preferential rise paths for the ascending bubbles. This phenomenon is typically termed channeling. Generally, the location of these preferential rise paths is not static due to the shifting of the fiber network caused by interaction with intermittent rising bubbles. For example, a small bubble may become trapped in a fiber network, but other rising bubbles may also get trapped and coalesce with the first bubble to form a resulting bubble large enough to break through the network. As it breaks through, the adjacent fibers are pushed aside, which may close a nearby preferential rise path and cause a new local fiber network to form. This new network will now trap bubbles in this region, and the process begins again. Therefore, the overall flow conditions within the column are more likely to be quasi-steady-state in nature.

As the bubbles rise from Position 1 to Position 2 in Fig. 3a, they become more dispersed, but there are still regions in the column deficient of bubbles. Bubble dispersion continues toward the top of the column with Position 3 showing the most uniform bubbly flow of the three locations recorded at this air injection rate.

Figure 3b reveals the resulting flow patterns for the air injection flow rate of 2.0 slpm with an ONP consistency of 1%. Considerable coalescence takes place under these conditions and the resulting flow patterns are considered to be churn-turbulent. Therefore, increasing the fiber consistency results in an early transition to churn-turbulent flow.

When the air injection rate is further increased to 15 slpm (Fig. 3c), a very chaotic flow pattern is recorded on the radiographs. Very large bubbles are observed due to the high coalescence rate. The resulting bubbles also vary in shape due to the highly turbulent nature of the flow field. In addition to the very large bubbles, some very small bubbles are also recorded. However, due to the small buoyant force associated with these bubbles, they are typically carried toward the column bottom due to backmixing. This is visually observed in the flow near the walls but not specifically recorded in the radiographs.

As shown in Fig. 4 for Position 2 and an air flow rate of 2 slpm, increasing the fiber consistency from 0 to 1.5% results in fewer but larger and more spherical bubbles recorded on the radiographs because the fibers enhance bubble coalescence. This is most significant for the given conditions at consistencies between 1.0% and 1.5%. The fewer, larger bubbles result in a significant reduction in the overall bubble surface area, which will be detrimental to any process where maximizing gas bubble surface area is important, such as flotation deinking or bleaching with gaseous chemicals.

2.3 Ongoing Bubble Visualization Research

Our initial FXR research has displayed that this flow visualization technique is a valuable tool to observe gas flows in opaque fiber suspensions. We have recently completed work using FXR to measure bubble size in an ONP suspension with a single air inlet comprised of a sparger or a small orifice in a gasket. Details of this research can be found in [20]. Additional FXR research that is currently underway includes investigating the effect of system chemistry, fiber type, and fiber length on bubble size. We are also pursuing research in other areas in a mill where the flow visualization of gas/liquid/fiber systems may provide valuable insight into the fluid flow conditions.

3. GAS HOLDUP MEASUREMENTS

Aeration ratios of 200-1000% have been reported for flotation deinking equipment [10]. This value is defined as the volumetric gas flow rate compared to the volumetric slurry flow rate, and is easily controlled or

altered by adjusting either (or both) flow rates. However, these values do not necessarily correlate to effective flotation cell operation. Gas holdup (or void volume or void fraction), defined as the percent gas volume in a multiphase system, may be a more appropriate measure for flotation cell performance. Gas holdup may be influenced by the flow conditions, flow geometry, and fiber consistency, and is typically spatially dependent. Typical flotation cells operate with a gas holdup on the order of 10-20% [21]. However, a high gas holdup is not necessarily better. A uniform gas holdup created by bubbly flow conditions would be more desirable in a flotation cell because the air being introduced into the system would be uniformly distributed. In general, to identify optimum operating conditions, the magnitude and distribution of gas holdup in a cell would be needed, with a high, but uniformly distributed, value being most desirable. We are currently performing gas holdup studies in gas/liquid/fiber systems.

3.1 Measuring Gas Holdup

Gas holdup in a multiphase system can be recorded with a variety of methods, including measuring the increase in column height when the gas is introduced [21, 22], dynamic gas disengagement [23], pressure drop measurements [22], electric resistivity probes [4, 24], and gamma densitometry [21, 24, 25]. Gamma densitometry is a radiation technique in which the attenuation of a gamma-ray beam (caused by mass interference) between a gamma source and detector is recorded and correlated to the chord-average gas holdup value. Details of this technique can be found in [21, 24-26]. This latter technique is being utilized at IPST to record gas holdup in fiber suspensions.

3.2 Gas Holdup in ONP Suspensions

Lindsay et al. [21] measured gas holdup in a cylindrical quiescent bubble column filled with 0, 1, and 2% ONP fiber suspensions. Gas holdup values were less uniform and lower in the fiber systems, implying gas channeling and lower gas residency time in the suspension. Both conditions are detrimental to effective flotation deinking. Lindsay et al. [21] also completed gas holdup experiments in a cocurrent bubble column filled with either 0 or 1% ONP fiber suspensions. In these experiments, the 1% fiber suspension had a higher gas holdup than that recorded for the water system, and the gas holdup increased when the superficial liquid velocity exceeded the superficial gas velocity. Here, the superficial velocity represents the effective liquid or gas velocity in the column if only one constituent is present and is defined as the liquid or gas volumetric flow rate divided by the column cross-sectional area.

An extension of this study has recently been completed in the identical cocurrent bubble column, which is depicted in Fig. 5 [26]. The bubble column was 1.5 m high with an interior diameter of 12.7 cm. Chord-averaged gas holdup values were determined at ten lateral and six vertical locations, while the superficial gas velocity (υ_g) was varied from $0.5 \leq \upsilon_g \leq 4.0$ cm/s, the superficial liquid velocity (υ_ℓ) was varied from $2.5 \leq \upsilon_\ell \leq 7.5$ cm/s, and unprinted ONP fiber suspensions of 0, 0.8 and 1.2% were considered.

Figure 6 displays typical chord-average gas holdup profiles obtained for the 0.8% ONP suspension, where the highest values were obtained in the center of the bubble column. As expected, increasing the superficial gas velocity increases the gas holdup for a fixed superficial liquid velocity and column height. This was observed for all pulp consistencies, column heights, and superficial liquid flow rates.

As air is injected into a bubble column, the bubbles rise from the injector ports. If the bubbles are not removed fast enough, they coalesce with other bubbles forming larger bubbles with a corresponding larger buoyant force and faster rise velocity. These large, fast rising bubbles tend to reduce the gas holdup when compared to well-dispersed small bubbles produced at the same air flow rate. For a fixed air flow rate, if the liquid flow rate in the bubble column increases, the faster flowing fluid removes bubbles from the injector port at a faster rate, which keeps the bubbles small and well-dispersed, as well as increases the amount of backmixing observed in the system. This results in an increase in the cross-sectional average gas holdup as the superficial velocity is increased. Figure 7 shows this trend for a column height of H = 50.8 cm for three superficial gas velocities (υ_g = 0.5, 2.0, and 4.0 cm/s) and all consistencies considered by Schulz [26]. It is interesting to note that the consistency at which the maximum cross-sectional average gas holdup occurs depends on both the liquid and gas superficial velocities.

This relationship is better depicted in Fig. 8 for a superficial gas velocity of 4.0 cm/s and a column height of 50.8 cm. For all considered conditions, the lowest cross-sectional average gas holdup occurs at an ONP consistency of 1.2%. When the superficial liquid velocity is 2.5 cm/s, the maximum cross-sectional average gas holdup occurs in the air/water system (0% consistency). However, when the superficial liquid velocity is 5.0 or 7.5 cm/s, the maximum cross-sectional average gas holdup occurs when the ONP

consistency is 0.8%. This interesting result will be further discussed in an upcoming publication [27].

3.3 Ongoing Gas Holdup Research

Gas holdup measurements are important to the pulp and paper industry and may not follow the trends typically observed in simple air/water systems. Therefore, we are interested in determining the effect of fiber type, fiber consistency, system chemistry, and flow conditions on gas holdup in fiber suspensions. These, and other important parameters, will be the focus of future research.

4. MIXING IN FIBER SUSPENSIONS

During the paper recycling process, mixing, either intentional or unintentional, occurs from the pulping to the papermaking process. For example, turbulence increases the mixing effectiveness in a pulp suspension, which will increase the number of bubble/particle collisions in a flotation cell. Depending on the process conditions (e.g., temperature, pH), the mixing rate may also alter the particle size of some stickie materials. We are addressing this issue by performing experiments in a mixing tank filled with various consistencies of fiber suspensions and a small amount (by volume) of a curtain coating wax.

4.1 The Mixing Tank

These experiments are conducted in a Standard Vessel Configuration (SVC) mixing tank [28, 29], where the impeller, baffles, and mixing chamber all have specific dimensions relative to one another. Figure 9 is a schematic of the SVC mixing tank used in our experiments, which is temperature controlled and has the ability for air injection below the impeller blades to simulate flotation.

Following the experimental procedures of Shinnar [30], tests are conducted by heating the tank to 60°C, which is above the melting point of the curtain coating wax (~54°C) that was added to the tank. A small amount of Poly Vinyl Alcohol (~500 ppm) was also added to the mixture as a suspending agent. The molten wax globules reach a steady-state particle size distribution that depends on the tank operating conditions, such as fiber consistency and mixing rate. Small liquid samples are then removed from the tank at specified locations and rapidly quenched in cold water to freeze the particle size in place. The effect of tank operating conditions on wax particle size distribution is then determined through image analysis of the resulting particles [30, 31]. The image analysis was performed by using a microscope at 80x magnification to determine the frontal areas and perimeters of all particles with perimeters larger than 31.4 μm. Wax particles with smaller perimeters were discarded because, in addition to consisting of a small fraction of all particles, they were often difficult to distinguish from the background. Equivalent particle diameters were then determined on the basis of particle projected area. Further details of this technique can be found in [31, 32].

4.2 Synthetic Fiber Results

Bose et al. [31] recently completed a series of mixing experiments using Nylon fibers. Fluid samples were taken from five tank locations and the impeller speed was varied from 400 to 900 RPM, corresponding to a tank Reynolds number based on impeller diameter of $3.6 \times 10^4 \leq Re_I \leq 8.1 \times 10^4$. Nylon fiber consistency was also varied from 0 to 1% by weight. The resulting particle size distributions were shown to be spatially homogeneous for all considered conditions in which the consistency was ≤ 0.8%, confirming local isotropic turbulent conditions within the mixing tank. At 1% Nylon, the tank was stratified with the molten wax confined to the top of the tank.

Figure 10 displays the particle size distributions for four different Nylon consistencies while the tank mixing speed is fixed at 500 RPM. The data points represent the percentage of particles in a particular size range, where at least 1100 particles were analyzed for each distribution. The particle size distribution in water (0%) is bimodal with the first peak around 20 μm and the second peak near 120 μm. The reason for the bimodality of the particle size distribution is currently unknown, but is has been reported by other investigators [33, 34]. Adding Nylon fiber to the mixing tank, even in such dilute amounts as 0.1% by weight, considerably alters the resulting particle size distributions. As shown, when Nylon fiber is present, a monomodal particle size distribution results, which covers a smaller particle size range as consistency increases. Increasing the consistency also results in a decrease in the average wax particle size.

Figure 11 shows the effect tank mixing speed has on the wax particle size distribution for a fiber consistency of 0.5%. Increasing the tank speed creates more uniform particle size distributions that shift to smaller average particle sizes. This result is clearly revealed when the average particle diameter is plotted as a function of tank mixing speed for four Nylon consistencies (Fig. 12). Increasing the tank mixing speed and Nylon fiber consistency both reduce the average wax particle size. However, differences between

the 0.5 and 0.8% results are small. The cause of the particle size reduction as the mixing speed is increased is due to higher shear conditions at the higher speeds, resulting in smaller particles. The particle size reduction due to increased fiber consistency is not clear, but it is hypothesized that the fibers prevent coalescence of the molten wax particles. Additionally, collisions between molten wax particles and fibers may result in enhanced particle breakup, yielding a smaller steady-state particle size distribution.

4.3 Ongoing Mixing Research

Some recycling processes may operate at or above the melting temperature of specific contaminants, such as wax. We are using this mixing research to understand what effect this has on these special contaminants, and are currently investigating if cellulose fibers alter the particle size in the same manner that Nylon fibers do.

5. FLOTATION MODELING

Flotation deinking is a separation process in which swarms of air bubbles are injected into a relatively low consistency pulp slurry so that hydrophobic contaminant particles attach to the hydrophobic bubble surface. After a stable bubble/particle aggregate forms, the rising bubble carries the contaminant to the surface where it is removed from the system. Although flotation cell designs vary with respect to their geometry, flow configurations, and operating parameters, they all operate on similar principles, which have recently been reviewed [35]. These fundamental principles have been applied to formulate a mathematical model of the flotation deinking process.

5.1 The Overall Flotation Model

The overall flotation deinking model is based on the common assumption (see, for example, [35]) that the flotation process is comprised of a series of microprocesses that must occur sequentially to achieve successful particle removal. These microprocesses involve capture (or collision) of the particle by the bubble, attachment of the particle to the bubble as it slides over the bubble surface, the creation of a three-phase contact, and the stabilization of the bubble/particle aggregate as it rises through the suspension. Each of these microprocesses has an associated probability that it will successfully occur, and are functions of the bubble and particle physical properties (e.g., diameter, density), the fluid properties (e.g., viscosity, surface tension), and the system properties (e.g., contact angle, turbulent energy density, bubble and particle concentration). These relationships were originally developed for mineral flotation and are described in detail elsewhere [35-38]. Only specific values used in this model are summarized below.

The model for the overall flotation process can be described by

$$\frac{dn_p^f}{dt} = -k_1 n_p^f n_B^f + k_2 n_B^a \tag{1}$$

where n_p^f corresponds to the number of free particles in a unit volume available to attach to a bubble, n_B^f is the number of bubbles in the unit volume that are available for particle attachment, and n_B^a represents the number of bubbles with particles attached to it in the unit volume. The first term on the right-hand side represents the overall probability that a free particle will successfully attach to a bubble that is initially free of particles and can be likened to the death of free particles in a population balance equation. The second term on the right-hand side is a measure of the probability that the bubble/particle aggregate will become unstable and split to yield a "new" free particle in the unit volume and represents a birth of free particles in a population balance equation. This term has not been explicitly included in previous flotation models (i.e., [10, 39-47]).

The kinetic constants k_1 and k_2 are positive numbers described by the various microprocess probabilities and the collision frequency:

$$k_1 = ZP_cP_{asl}P_{tpc}P_{stab} \tag{2}$$

$$k_2 = Z'P_{destab} = Z'(1 - P_{stab}) \tag{3}$$

In Eq. (2), Z is related to the collision frequency which we take to have the form implied by the work of Liepe and Möckel [48], namely,

$$Z = 2^{7/9}\frac{5}{3}\left(\frac{\varepsilon^{4/9}}{\nu_\ell^{1/3}\rho_\ell^{2/3}}\right)\left(R_p + R_B\right)^2 \times\left(R_p^{14/9}\Delta\rho_p^{4/3} + R_B^{14/9}\Delta\rho_B^{4/3}\right)^{1/2} \tag{4}$$

where ν_ℓ and ρ_ℓ are the fluid kinematic viscosity and fluid density, respectively, ε is the turbulent energy density, R_p and R_B are the particle and bubble radius, $\Delta\rho_p = \rho_p - \rho_\ell$, $\Delta\rho_B = \rho_B - \rho_\ell$, and ρ_p and ρ_B are the particle and bubble density. Equation (4) would be applicable to flotation cells with agitation. Note that this expression differs from that presented in [36] by a factor of $n_B n_p$, where n_B and n_p are the total number of bubbles and particles per unit volume. The original expression in [36] was adopted following the work of Schulze [49, 50]. However, as recently pointed out by Julien Saint Amand [10], the Z in Eq. (2) should not

have the $n_B n_p$ term because it accounts for the collisions between free particles (n_p^f) and free bubbles (n_B^f), which are already incorporated into Eq. (1). Therefore, $Z n_p^f n_B^f$ is a true collision frequency with units of number per unit time per unit volume.

In Eq. (2), P_c represents the probability of collision and is described by the expression from Yoon and Luttrell [51]

$$P_c = \left[\frac{3}{2} + \frac{4 Re_B^{0.72}}{15}\right]\left(\frac{R_p}{R_B}\right)^2 \tag{5}$$

where Re_B is the bubble Reynolds number defined by

$$Re_B = \frac{\upsilon_B d_B \rho_\ell}{\mu_\ell} \tag{6}$$

where υ_B is the bubble rise velocity, $d_B = 2R_B$, and μ_ℓ is the fluid dynamic viscosity. The probability of attachment by sliding (P_{asl}) is determined from the formulation of Schulze [40]

$$P_{asl} = \sin^2 \phi^*_{crit} \tag{7}$$

where ϕ^*_{crit} is the critical position angle that may be determined only by numerically solving the system of ordinary differential equations which govern the adhesion by sliding process [40]. This process is also discussed in detail in [35]. The probability of three-phase contact (P_{tpc}) is assumed to be approximately one (i.e., $P_{tpc} \approx 1$). The probability of stability (P_{stab}) is determined from [40, 52]

$$P_{stab} = 1 - \exp\left(1 - \frac{1}{Bo'}\right) \tag{8}$$

where

$$Bo' = \frac{F_{detachment}}{F_{attachment}} \tag{9}$$

with

$$F_{detachment} = 4R_p^2\left(\Delta\rho_p g + \frac{1.9\rho_p \varepsilon^{2/3}}{(R_p + R_B)^{1/3}}\right) + 3R_p\left(\frac{2\sigma}{R_B} - 2R_B\rho_\ell g\right)\sin^2\left(\pi - \frac{\theta}{2}\right) \tag{10}$$

and

$$F_{attachment} = \left|6\sigma \sin\left(\pi - \frac{\theta}{2}\right)\sin\left(\pi + \frac{\theta}{2}\right)\right| \tag{11}$$

where g is the acceleration due to gravity, σ is the surface tension, and θ is the contact angle.

Based on new research, k_2 in Eq. (3) is slightly different from that previously presented (i.e., [36]). Based on dimensional considerations, k_2 should have units of 1/time, giving the second term on the right-hand side of Eq. (1) the units of number per unit time per unit volume, which is consistent with the other terms. Since P_{destab} (or P_{stab}) is a true probability and is unitless, an additional term has to be included in k_2, which we call Z' and has units of 1/time. This term could be thought of as a collision rate between bubble/particle aggregates and the "thing" that makes the aggregate unstable, like a turbulent eddy. Current research is directed toward quantifying this term.

As a first estimate, we argue that $k_2 \leq 1$, based on the reasoning that at most, the number of free particles that could be generated at a given instant in time due to the destabilization of the bubble/particle aggregate is equivalent to n_B^a, the number of bubbles per unit volume with attached particles at that instant in time. This assumes that only one particle could attach to a bubble, an assumption we are currently relaxing. Therefore, values of $k_2 > 1$ have no physical meaning. Since $0 \leq P_{destab} \leq 1$, $Z'P_{destab} \leq 1$. As a first approximation, we will assume that $Z' = 1$ (and has the appropriate units of 1/time). This assumption will be modified as we continue to research this area.

Using the appropriate values for k_1 and k_2 outlined above, Eq. (1) can be solved to predict flotation efficiency as a function of time, the flotation efficiency for a fixed flotation time, and the time period to reduce the number of free particles in the unit volume by a factor of two. An example of one such plot, based on model predictions, of the flotation efficiency for a fixed flotation time of 600 seconds (10 minutes) is shown in Fig. 13. This figure was generated with the fluid properties corresponding to those of water and the following parameters fixed: υ_B = 10 cm/s, ρ_p = 1.3 g/cm^3, σ = 50 dynes/cm, $\theta = 60°$, ε = 10 W/kg, $\phi^*_{crit} = 60°$, n_B = 1000, and n_p = 100. It is known that surface tension and turbulent energy density affect bubble size [49, 53-55], but the specific relationship may be system dependent. We also know that the bubble rise velocity will be a function of bubble radius [3], but this relationship is unknown for fiber suspensions. In the calculations presented here, we have held both σ and υ_B fixed and present Fig. 13 as an example of the type of results that can be predicted with our model.

Figure 13 reveals that the efficiency is not very good for the indicated conditions. We believe this is the result of two assumptions we initially incorporated into the model: a bubble can have only one particle attached to it, and the total number of bubbles in a unit volume

must be greater than the total number of particles. In actual flotation units, these assumptions are not likely to be true and the results presented here would provide the lowest efficiency predictions. We are currently addressing modifications to our first-generation model (Eq. (1)) to relax these assumptions.

Figure 13 does reveal that for the two bubble radii considered, small particles are not removed very effectively. Increasing the particle radius results in an increase in the efficiency until a maximum is reached, which depends on the bubble radius, then the efficiency declines toward zero because the bubble/particle aggregate becomes unstable. The shape of these curves is similar to those typically presented when flotation efficiency is plotted as a function of particle size, where flotation is performed for a given time period [56, 57]. Therefore, at least qualitatively, the model predicts what is typically observed in industry.

5.2 Current Modeling Research

The purpose of a flotation deinking model is to be able to predict separation efficiencies and general performance trends before full-scale experiments and mill trials are performed. However, model validation studies must be completed to determine the model effectiveness at predicting flotation performance. These studies are currently underway at IPST. In conjunction with model validation experiments, model improvements, as alluded to above, are also being addressed.

The microprocess probabilities that are incorporated in the model kinetic constants, k_1 and k_2, and adopted from the mineral processing industry, also include specific assumptions. Details of these assumptions are found in [35]. Our current research is focusing on the probability of collision and the probability of attachment by sliding, where we are developing a more accurate model and a closed-form approximation for these expressions, respectively.

6. CONCLUSIONS

Flotation deinking is a very complex separation process. A considerable effort is being coordinated at the Institute of Paper Science and Technology to understand the relevant fluid mechanic issues involved in effective flotation. A technique to visualize gas flows in fiber suspensions at typical flotation deinking operating consistencies has provided great insight into what occurs in a fiber suspension when gas is injected. Bubble size measurements from the resulting images are possible, and are being used to determine how bubble size changes when specific flotation conditions are altered. Gas holdup measurements in a cocurrent bubble column are also being used to determine what affects this quantity. Current areas of interest include fiber consistency and fiber type. Mixing is also important for effective flotation deinking, and we are addressing what effect mixing has on contaminant size in a fiber suspension. Finally, a mathematical model of the flotation macroprocess has been developed from the flotation microprocesses that govern the formation of a stable bubble/particle aggregate. Model validation and relaxation of specific restrictions are currently being investigated.

This research covers various topics and can be generalized to improving our understanding of gas/liquid/fiber/particle flows. The fluid mechanics of this type of system are very important to effective flotation deinking. This information can also be applied to other recycling unit operations, as well as bleaching with gaseous chemicals, direct contact steam heating, and air removal from fiber suspensions.

7. ACKNOWLEDGMENTS

This work was funded by the Member Companies of the Institute of Paper Science and Technology. Their continued support is greatly appreciated. Many other individuals also contributed to this research effort and include Dr. F. Bloom, Dr. M. Ghiaasiaan, Dr. K. Maruvada, Mr. P. Phelan, Ms. A. Emery, Mr. J. Monefeldt, Mr. T. Schulz, Mr. F. Bose, Mr. S. Omberg, and Mr. G. Smith.

8. BIBLIOGRAPHY

[1] Hutten, E.M., and Banerjee, S., "Fiber:Water Distribution of Stickies," *Paper Recycling Challenge - Stickies*, M.R. Doshi, and J.M. Dyer, Eds., Appleton, WI, Doshi & Associates Inc., 33-39 (1997).

[2] Deng, Y., "Flotation Deinking Chemistry: The Current Research Program at IPST," *Paper Recycling Challenge: Vol. III - Process Technology*, M.R. Doshi, and J.M. Dyer, Eds., Appleton, WI, Doshi & Associates, Inc., (1998).

[3] Clift, R., Grace, J.R., and Weber, M.E., *Bubble, Drops, and Particles*, Academic Press, New York, 1978.

[4] Hetsroni, G., Ed. *Handbook of Multiphase Systems*, Hemisphere Publishing Corp., New York, 1982.

[5] Shook, C.A., and Roco, M.C., *Slurry Flow: Principles and Practice*, Butterworth-Heinemann, Boston, 1991.

[6] Saxena, S.C., Patel, D., Smith, D.N., and Ruether, J.A., "An Assessment of Experimental Techniques for the Measurement of Bubble Size in a Bubble Slurry Reactor as Applied to Indirect Coal Liquefaction," *Chemical Engineering Communications*, **63**: 87-127 (1988).

[7] Zhu, J.Y., "Laser Doppler Velocimetry for Flow Measurements in Pulp and Paper Research," *1996 Engineering Conference*, Chicago, TAPPI Press, 3-18 (September 16-19, 1996).

[8] Walmsley, M.R.W., "Air Bubble Motion in Wood Pulp Fibre Suspension," *APPITA 1992 Proceedings*, 509-515 (1992).

[9] Hunold, M., Krauthauf, T., Müller, J., and Putz, H.-J., "Effect of Air Volume and Air Bubble Size Distribution on Flotation in Injector Aerated Deinking Cells," *Journal of Pulp and Paper Science*, **23**(12): J555-J560 (1997).

[10] Julien Saint Amand, F., "Hydrodynamics of Flotation: Experimental Studies and Theoretical Analysis," *1997 TAPPI Recycling Symposium*, Atlanta, GA, TAPPI Press, 219-241 (1997).

[11] Farrington, T.E., Jr., "A More Fundamental Approach to the Problem of High Consistency Forming," *1986 TAPPI Engineering Conference*, Atlanta, GA, TAPPI Press, 709-717 (September 22-25, 1986).

[12] Farrington, T.E., Jr., "Soft X-ray Imaging Can Be Used To Assess Sheet Formation and Quality," *TAPPI Journal*, **71**(5): 140-144 (1988).

[13] Farrington, T.E., Jr., "Flash X-ray Imaging of Kraft Black Liquor Sprays," *TAPPI Journal*, **71**(2): 89-92 (1988).

[14] Triantafillopoulos, N.G., and Farrington, T.E., Jr., "Flash X-ray Radiography Techniques for Visualizing Coating Flows," *1988 TAPPI Coating Conference*, New Orleans, LA, TAPPI Press, 47-52 (May 8-12, 1988).

[15] Zavaglia, J.C., and Lindsay, J.D., "Flash X-ray Visualization of Multiphase Flow During Impulse Drying," *TAPPI Journal*, **72**(9): 79-85 (1989).

[16] Monefeldt, J.L., "Flow Structures in a Quiescent Rectangular Bubble Column," Masters Thesis, Institute of Paper Science and Technology, Atlanta, GA (1996).

[17] Heindel, T.J., and Monefeldt, J.L., "Flash X-ray Radiography for Visualizing Gas Flows in Opaque Liquid/Fiber Suspensions," *6th International Symposium on Gas-Liquid Two-Phase Flows*, Vancouver, BC, ASME Press (June 22-26, 1997).

[18] Heindel, T.J., and Monefeldt, J.L., "Observations of the Bubble Dynamics in a Pulp Suspension Using Flash X-ray Radiography," *1997 TAPPI Engineering & Paper Makers Super Conference*, Atlanta, GA, TAPPI Press, 1421-1427 (1997).

[19] Hewitt, G.F., "Flow Regimes," *Handbook of Multiphase Systems*, G. Hetsroni, Ed., New York, Hemisphere Publishing Corp., Chapter 2.1 (1982).

[20] Heindel, T.J., "Bubble Size Measurements in a Fiber Suspension," *Journal of Pulp and Paper Science*, In Review (1998).

[21] Lindsay, J.D., Ghiaasiaan, S.M., and Abdel-Khalik, S.I., "Macroscopic Flow Structure in a Bubbling Paper Pulp-Water Slurry," *Industrial and Engineering Chemistry Research*, **34**: 3342-3354 (1995).

[22] Smith, J.S., Burns, L.F., Valsaraj, K.T., and Thibodeaux, L.J., "Bubble Column Reactors for Wastewater Treatment. 2. The Effect of Sparger Design on Sublation Column Hydrodynamics in the Homogeneous Flow Regime," *Industrial and Engineering Chemistry Research*, **35**: 1700-1710 (1996).

[23] Krishna, R., de Swart, J.W.A., Ellenberger, J., Martina, G.B., and Maretto, C., "Gas Holdup in Slurry Bubble Columns: Effect of Column Diameter and Slurry Concentrations," *AIChE Journal*, **43**(2): 311-316 (1997).

[24] Hewitt, G.F., *Measurement of Two Phase Flow Parameters*, Academic Press, New York, 1978.

[25] Torczynski, J.R., Adkins, D.R., Shollenberger, K.A., and O'Hern, T.J., "Application of Gamma Densitometry Tomography to Determine Phase Spatial Variation in Two-Phase and Three-Phase Bubbly Flows," *1996 Fluids Engineering Division Conference*, New York, ASME Press, 503-508 (1996).

[26] Schulz, T.H., "A Study of Gas Holdup in a Three-Phase Fibrous System," Masters Thesis, Institute of Paper Science and Technology, Atlanta, GA (1997).

[27] Schulz, T.H., and Heindel, T.J., "A Study of Gas Holdup in a Cocurrent Air/Water/Fiber System," In Preparation (1998).

[28] Tatterson, G.B., *Fluid Mixing and Gas Dispersion in Agitated Tanks*, McGraw-Hill, Inc., New York, 1991.

[29] Holland, F.A., and Chapman, F.S., *Liquid Mixing and Processing in Stirred Tanks*, Reinhold, New York, 1966.

[30] Shinnar, R., "On the Behaviour of Liquid Dispersions in Mixing Vessels," *Journal of Fluid Mechanics*, **10**: 259-275 (1961).

[31] Bose, F., Ghiaasiaan, S.M., and Heindel, T.J., "Hydrodynamics of Dispersed Liquid Droplets in Agitated Synthetic Fibrous Slurries," *Industrial and Engineering Chemistry Research*, **36**(11): 5028-5036 (1997).

[32] Bose, F., "Hydrodynamics of Dispersed Liquid Droplets in Agitated Synthetic Fibrous Slurries," Masters Thesis, Georgia Institute of Technology, Atlanta, GA (1997).

[33] Tobin, T., Muralidhar, R., Wright, H., and Ramkrishna, D., "Determination of Coalescence Frequencies in Liquid-Liquid Dispersions: Effect of Drop Size Dependence," *Chemical Engineering Science*, **45**(12): 3491-3504 (1990).

[34] Chatzi, E.G., Boutris, C.J., and Kiparissides, C., "On-Line Monitoring of Drop Size Distributions in Agitated Vessels. 1. Effects of Temperature and Impeller Speed," *Industrial and Engineering Chemistry Research*, **30**: 536-543 (1991).

[35] Heindel, T.J., "The Fundamentals of Flotation Deinking," *1997 TAPPI Pulping Conference*, San Francisco, CA, TAPPI Press, 521-533 (October 19-23, 1997).

[36] Heindel, T.J., and Bloom, F., "New Measures for Maximizing Ink Particle Removal in a Flotation Cell," *1997 TAPPI Recycling Symposium*, Atlanta, GA, TAPPI Press, 101-113 (1997).

[37] Bloom, F., and Heindel, T.J., "Mathematical Modelling of the Flotation Deinking Process," *Mathematical and Computer Modelling*, **25**(5): 13-58 (1997).

[38] Bloom, F., and Heindel, T.J., "A Theoretical Model of Flotation Deinking Efficiency," *Journal of Colloid and Interface Science*, **190**: 182-197 (1997).

[39] Schulze, H.J., *Physico-chemical Elementary Processes in Flotation*, Elsevier, Berlin, 1984.

[40] Schulze, H.J., "Flotation as a Heterocoagulation Process: Possibilities of Calculating the Probability of Flotation," *Coagulation and Flocculation*, B. Dobias, Ed., 321-353 (1993).

[41] Plate, H., and Schulze, H.J., "Modeling of the Overall Flotation Process Based on Physico-Chemical Microprocesses - Technique and Application," *XVII International Mineral Processing Congress*, Dresden, 365-377 (September 23-28, 1991).

[42] Sutherland, K.L., "Kinetics of the Flotation Process," *Journal of Physical Chemistry*, **52**: 394-425 (1948).

[43] Woodburn, E.T., "Mathematical Modelling of Flotation Processes," *Mineral Science and Engineering*, **2**: 3-17 (1970).

[44] Dorris, G.M., and Pagé, M., "Deinking of Toner-Printed Papers. Part I: Flotation Kinetics, Froth Stability and Fibre Entrainment," *3rd Research Forum on Recycling*, Vancouver, BC, 215-225 (November 20-22, 1995).

[45] Ahmed, N., and Jameson, G.J., "Flotation Kinetics," *Mineral Processing and Extractive Metallurgy Review*, **5**: 77-99 (1989).

[46] Pan, R., Paulson, F.G., Johnson, D.A., Bousfield, D.W., and Thompson, E.V., "A Global Model for Predicting Flotation Efficiency Part I: Model Results and Experimental Studies," *TAPPI Journal*, **79**(4): 177-185 (1996).

[47] Schmidt, D.C., and Berg, J.C., "The Effect of Particle Shape on the Flotation of Toner Particles," *Progress in Paper Recycling*, **5**(2): 67-77 (1996).

[48] Liepe, F., and Möckel, O.H., "Untersuchengen zum Stoffvereinigen in flüssiger Phase," *Chemical Technology*, **30**: 205-209 (1976).

[49] Schulze, H.J., "Zur Hydrodynamik der Flotations-Elementarvorgänge," *Wochenblatt Für Papierfabrikation*, **122**(5): 160, 162, 164-168 (1994).

[50] Schulze, H.J., "The Fundamentals of Flotation Deinking in Comparison to Mineral Flotation," *1st Research Forum on Recycling*, Toronto, Ontario, 161-167 (October 29-31, 1991).

[51] Yoon, R.H., and Luttrell, G.H., "The Effect of Bubble Size on Fine Particle Flotation," *Mineral Processing and Extractive Metallurgy Review*, **5**: 101-122 (1989).

[52] Hou, M.J., and Hui, S.H., "Interfacial Phenomena in Deinking I. Stability of Ink Particle - Air Bubble Aggregates in Flotation Deinking," *1993*

Pulping Conference, Atlanta, GA, TAPPI Press, 1125-1142 (1993).

[53] Sprow, F.B., "Distribution of Drop Sizes Produced in Turbulent Liquid-Liquid Dispersion," *Chemical Engineering Science*, **22**: 435-442 (1967).

[54] Hinze, J.O., "Fundamentals of the Hydrodynamic Mechanism of Splitting up in Dispersion Processes," *AIChE Journal*, **1**: 289 (1955).

[55] Tsouris, C., and Tavlarides, L.L., "Breakage and Coalescence Models for Drops in Turbulent Dispersions," *AIChE Journal*, **40**(3): 395-406 (1994).

[56] Ferguson, L.D., "Flotation Deinking Technology," *1995 Deinking Short Course*, Vancouver, WA, TAPPI Press, Chapter 10 (June 4-7, 1995).

[57] Vidotti, R.M., Johnson, D.A., and Thompson, E.V., "Hydrodynamic Particle Volume and its Relationship to Mixed Office Waste Paper Flotation Efficiency, Part 1," *1995 Pulping Conference*, Atlanta, TAPPI Press, 203-213 (1995).

9. FIGURES

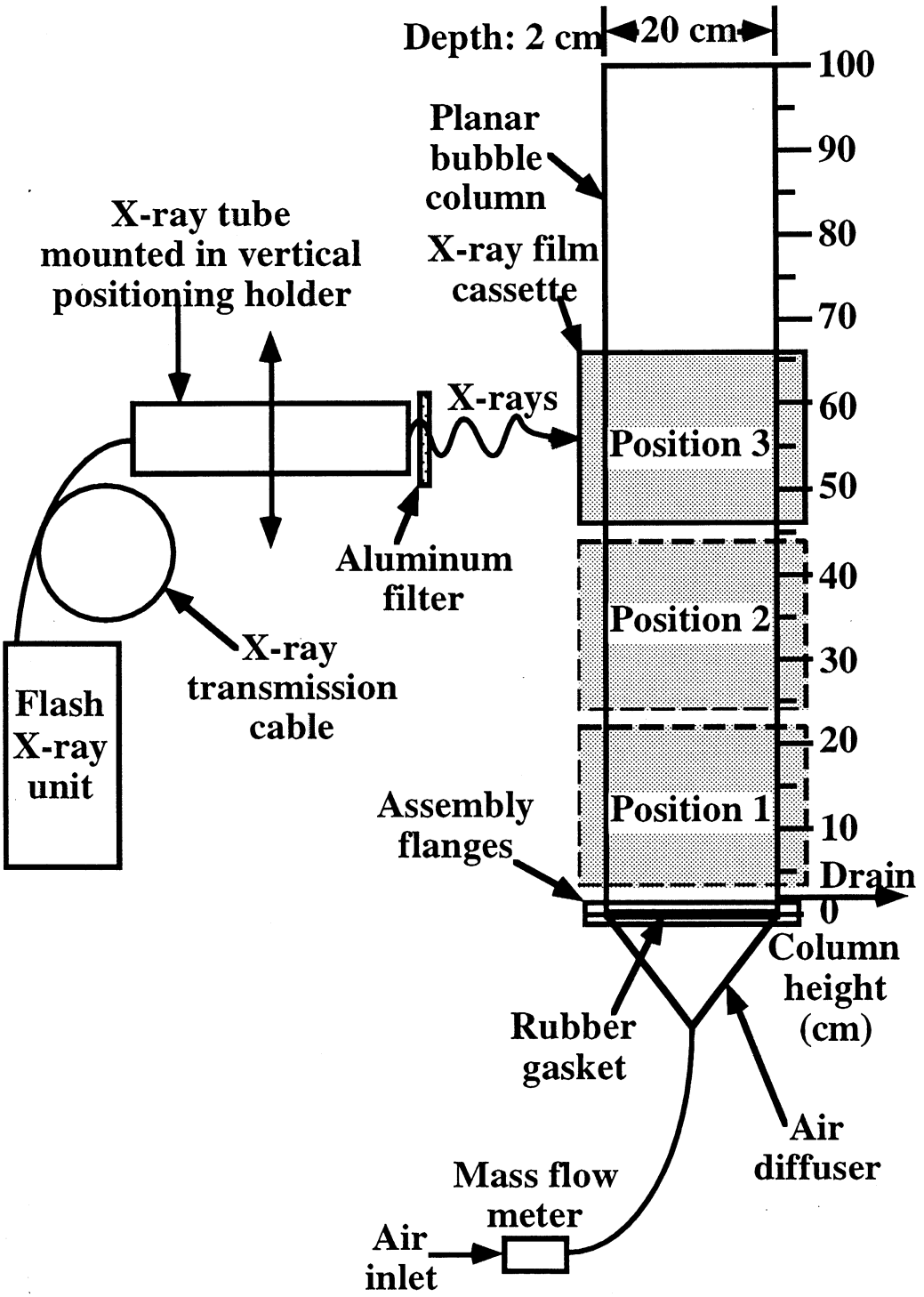

Figure 1: Schematic diagram of the IPST flash x-ray radiography experimental set up.

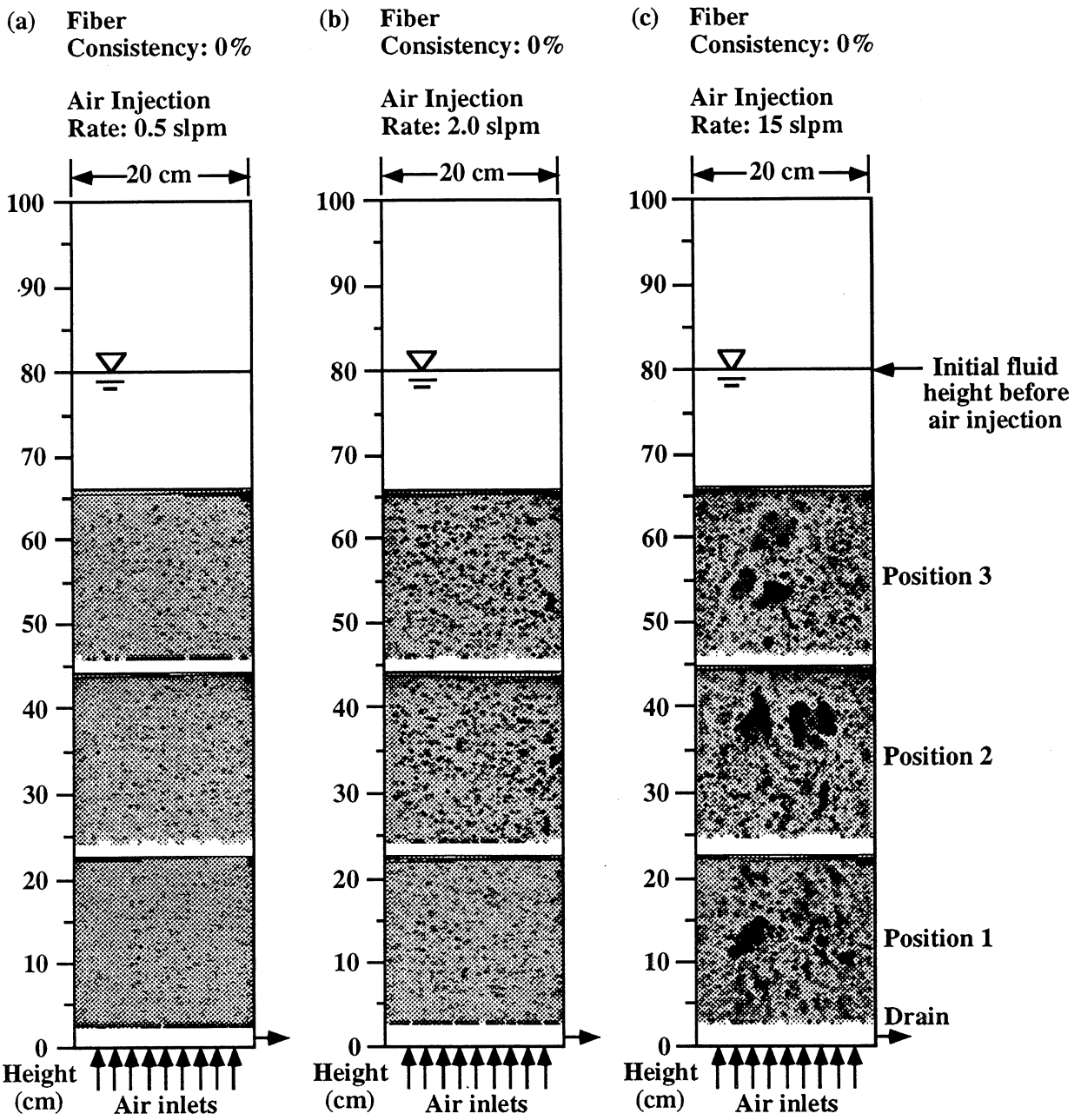

Figure 2: Radiograph composite of the bubble flow patterns (the dark regions represent air bubbles) in an air/water system at air injection rates of (a) 0.5 slpm, (b) 2.0 slpm, and (c) 15 slpm.

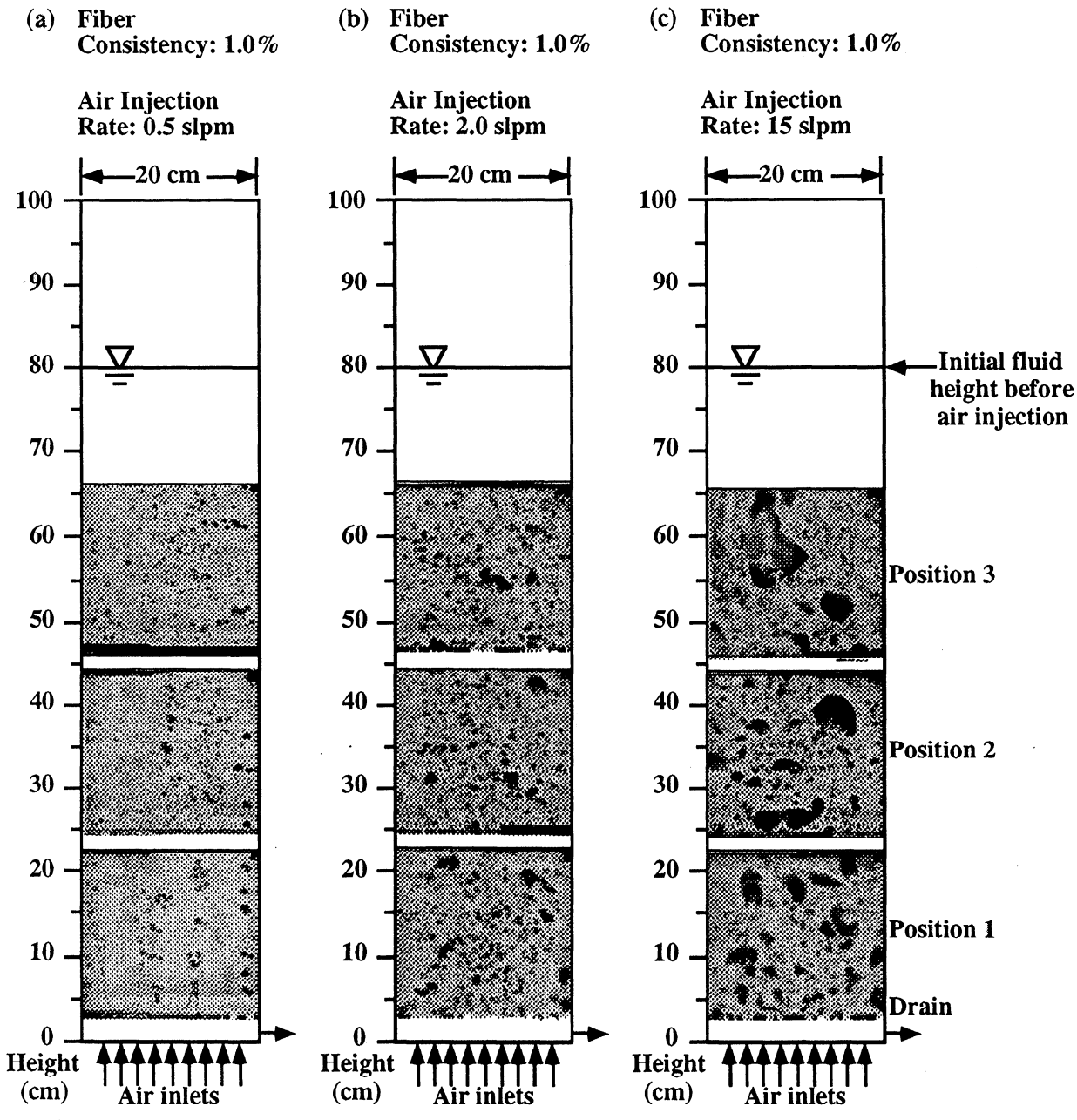

Figure 3: Radiograph composite of the bubble flow patterns (the dark regions represent air bubbles) in an air/water/1% ONP system at air injection rates of (a) 0.5 slpm, (b) 2.0 slpm, and (c) 15 slpm.

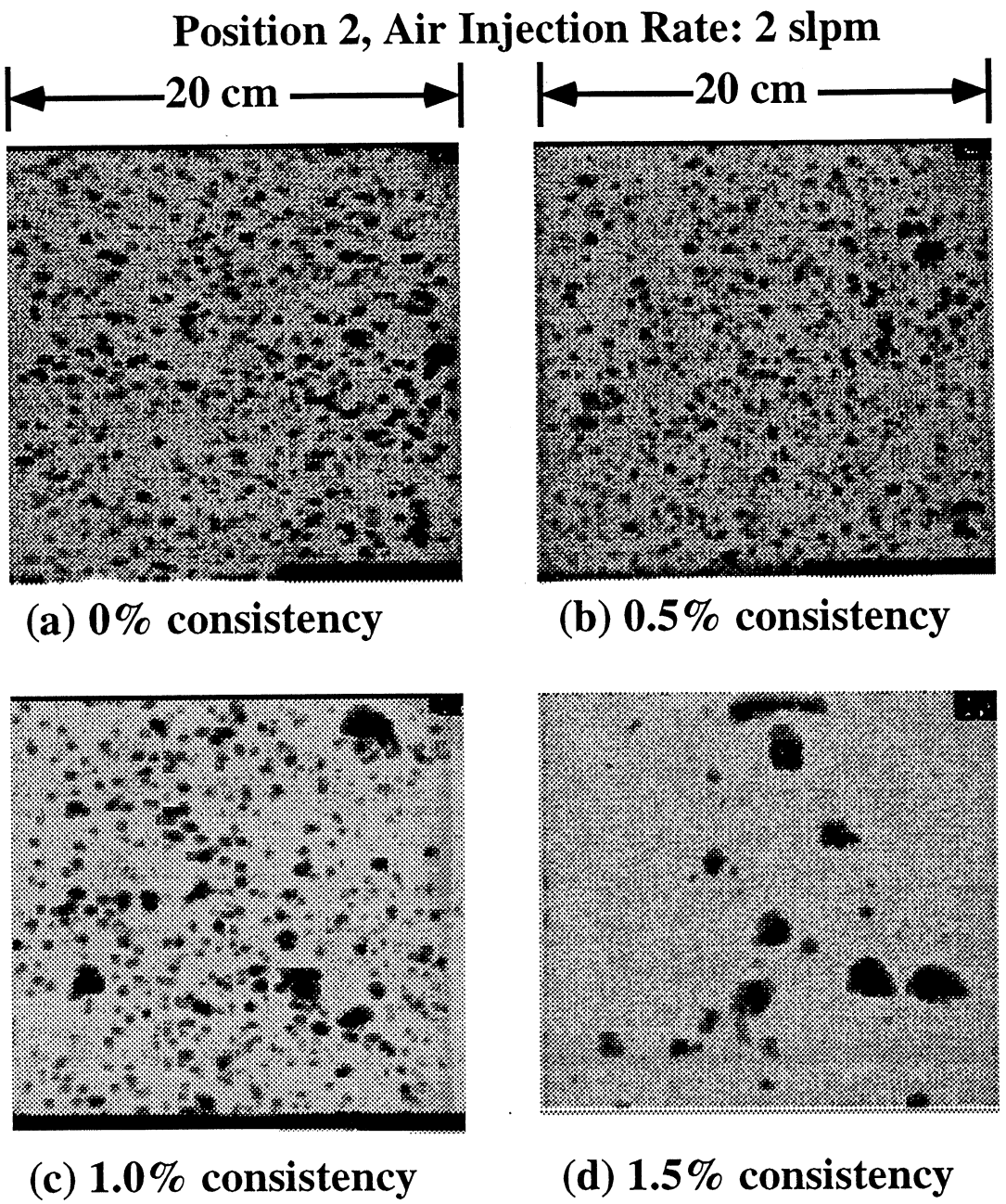

Figure 4: Effect of fiber consistency on air bubble flow patterns at Position 2 and an air injection rate of 2 slpm.

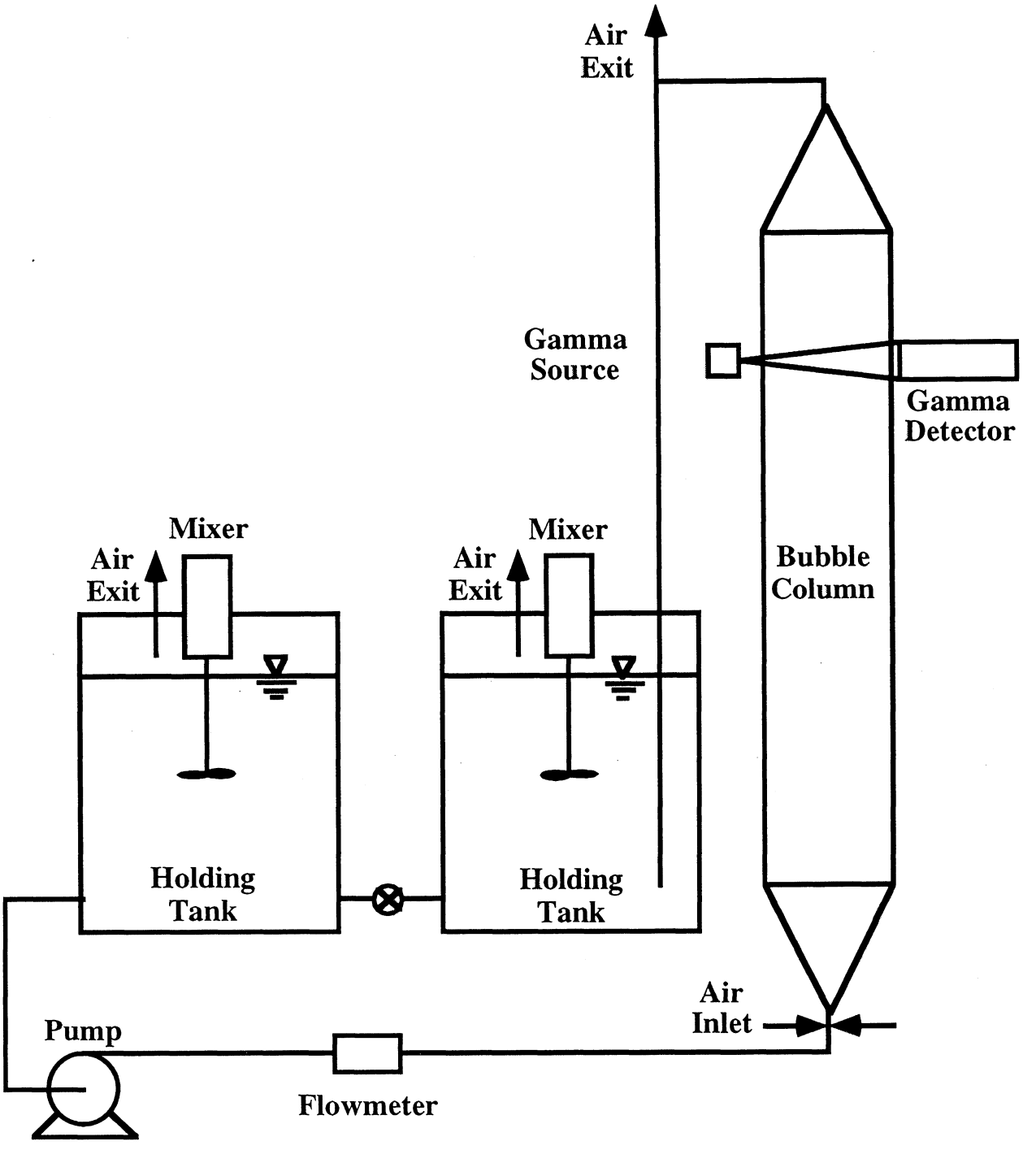

Figure 5: Schematic diagram of the IPST cocurrent bubble column used for gas holdup measurements.

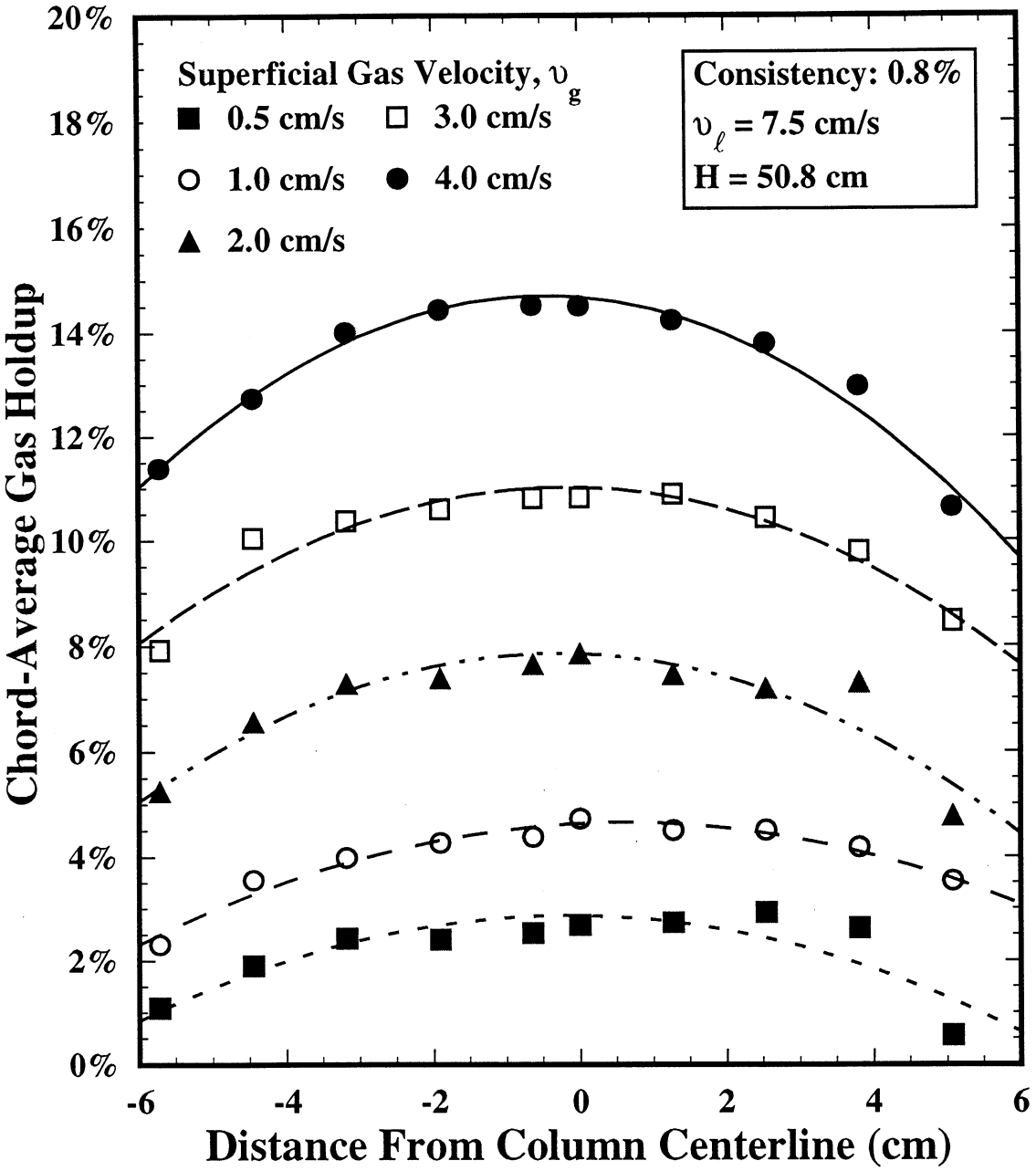

Figure 6: Chord-average gas holdup measurements at a column height of H = 50.8 cm for various superficial gas velocities, a superficial liquid velocity of 7.5 cm/s, and an ONP consistency of 0.8%.

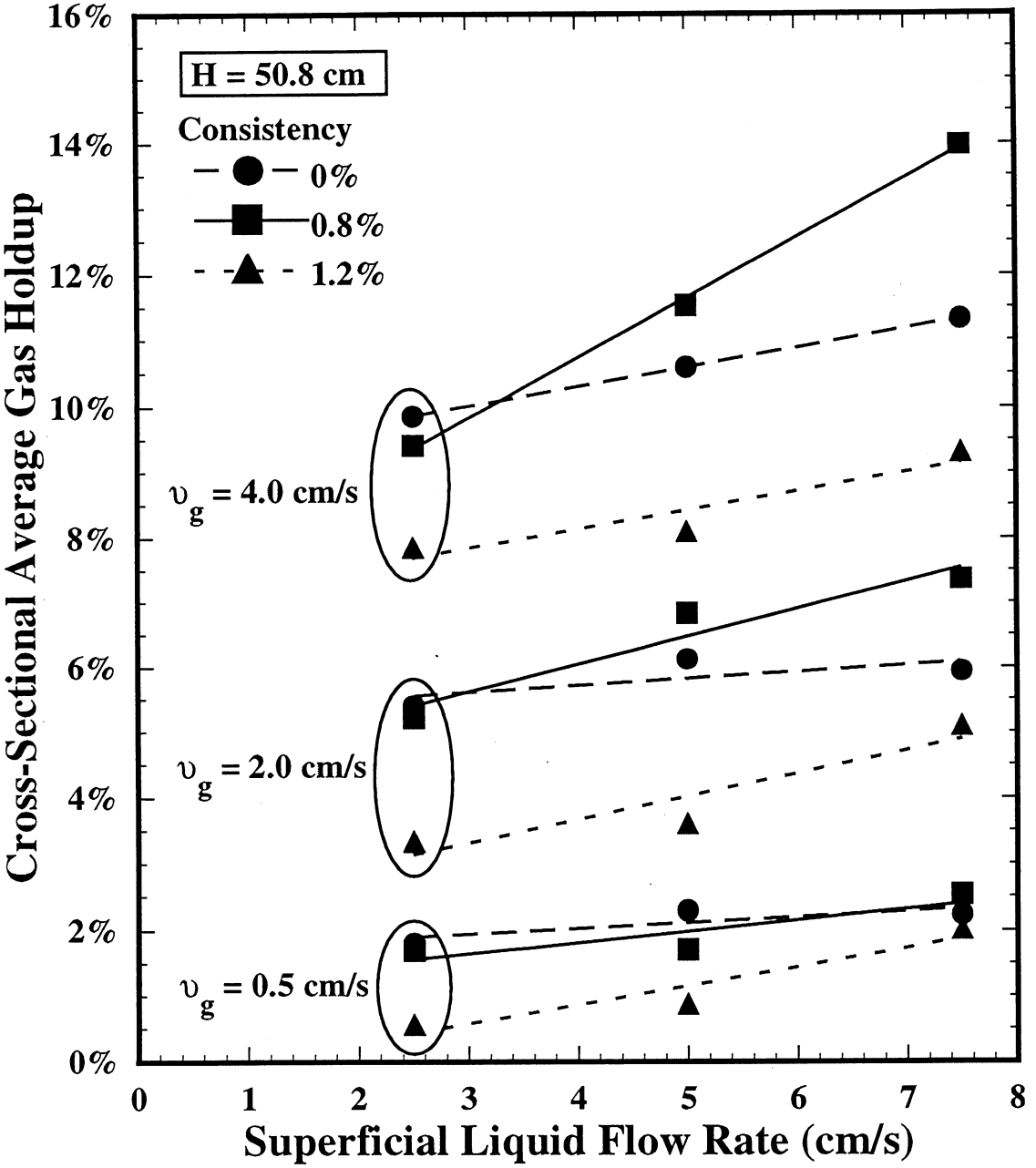

Figure 7: Cross-sectional average gas holdup measurements at a column height of H = 50.8 cm for various ONP consistencies and superficial liquid and gas velocities.

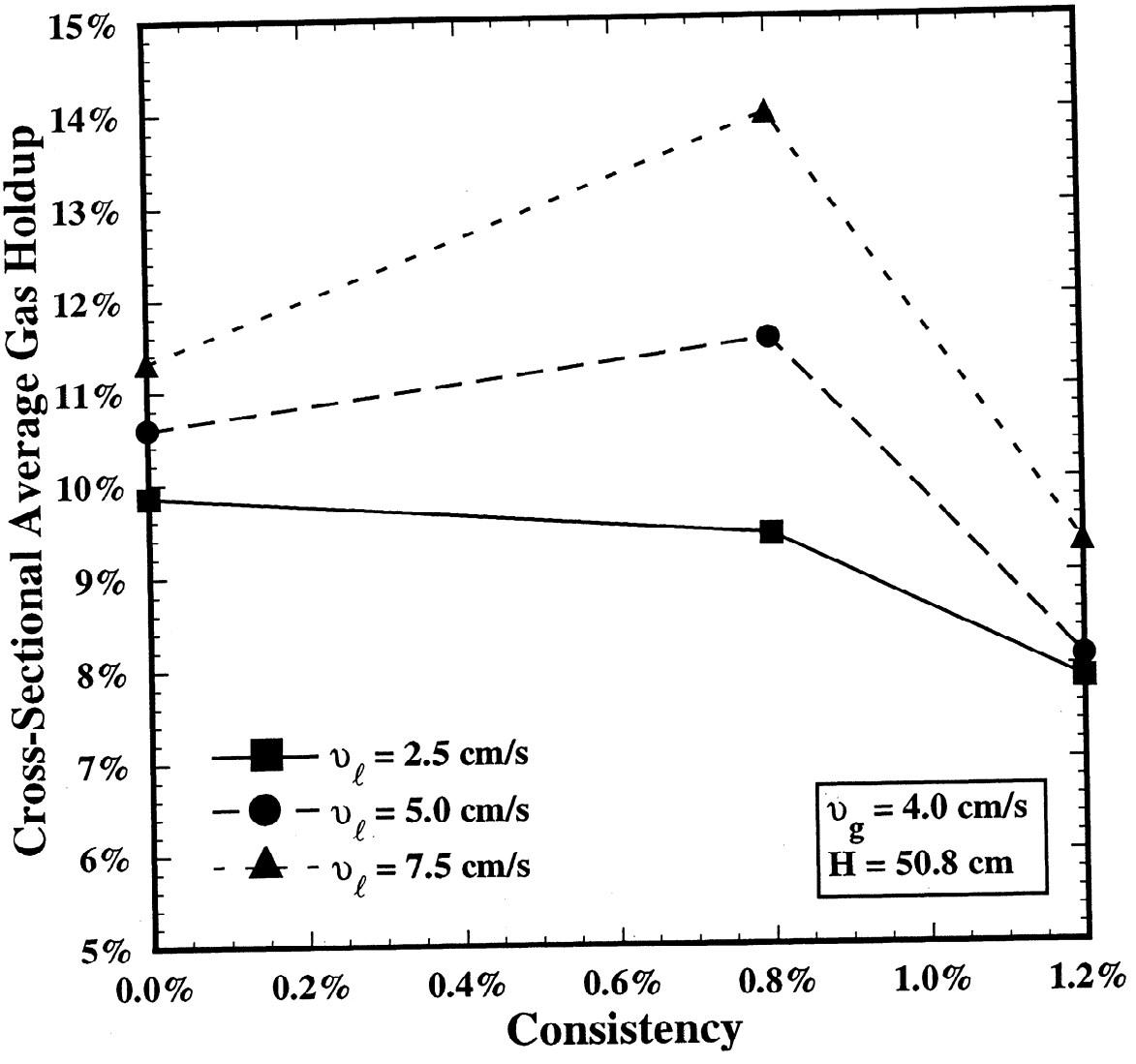

Figure 8: Cross-sectional average gas holdup measurements as a function of ONP consistency for a superficial gas velocity of 4.0 cm/s and a column height of 50.8 cm.

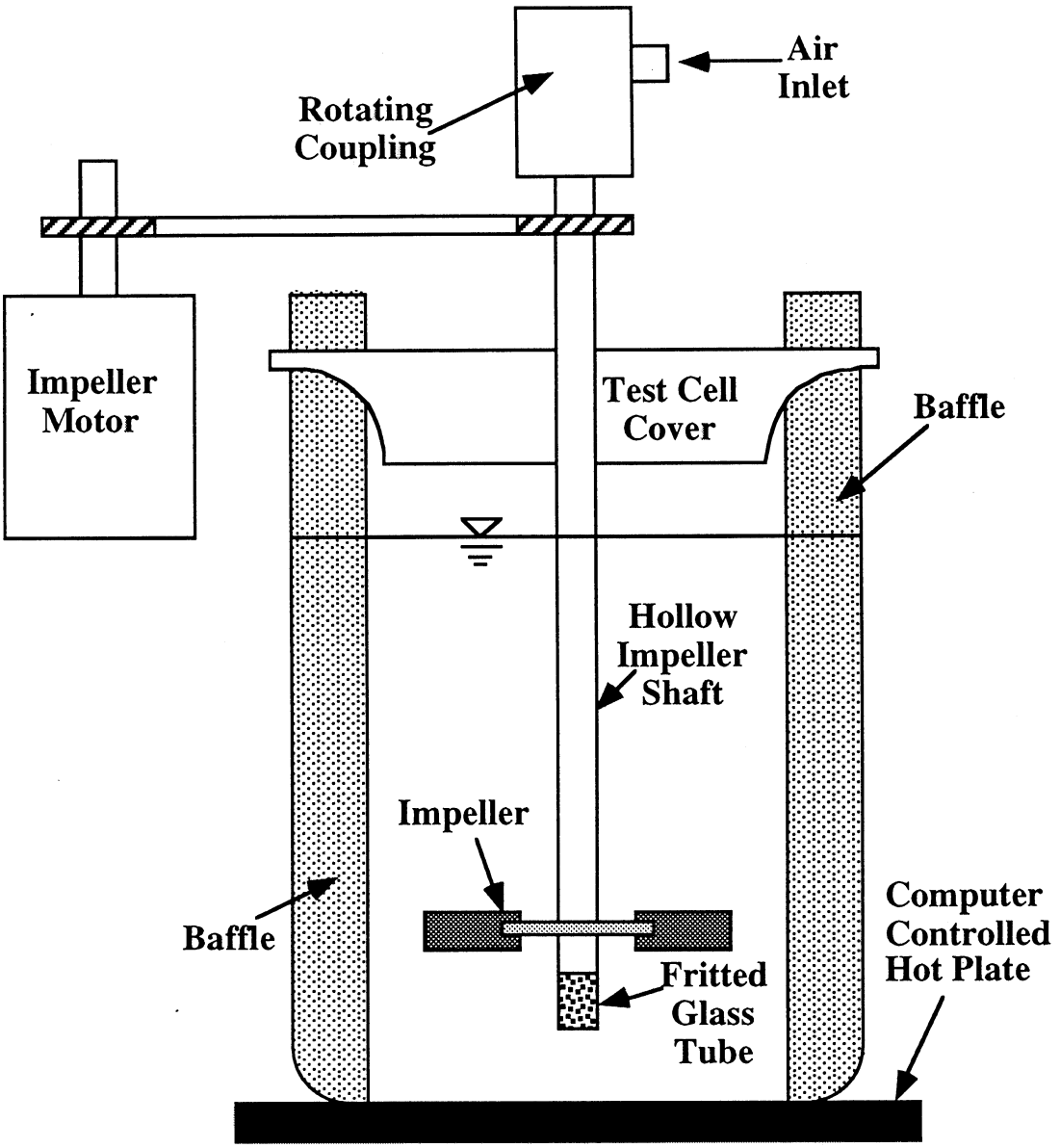

Figure 9: Schematic diagram of the SVC mixing tank used in the IPST experiments.

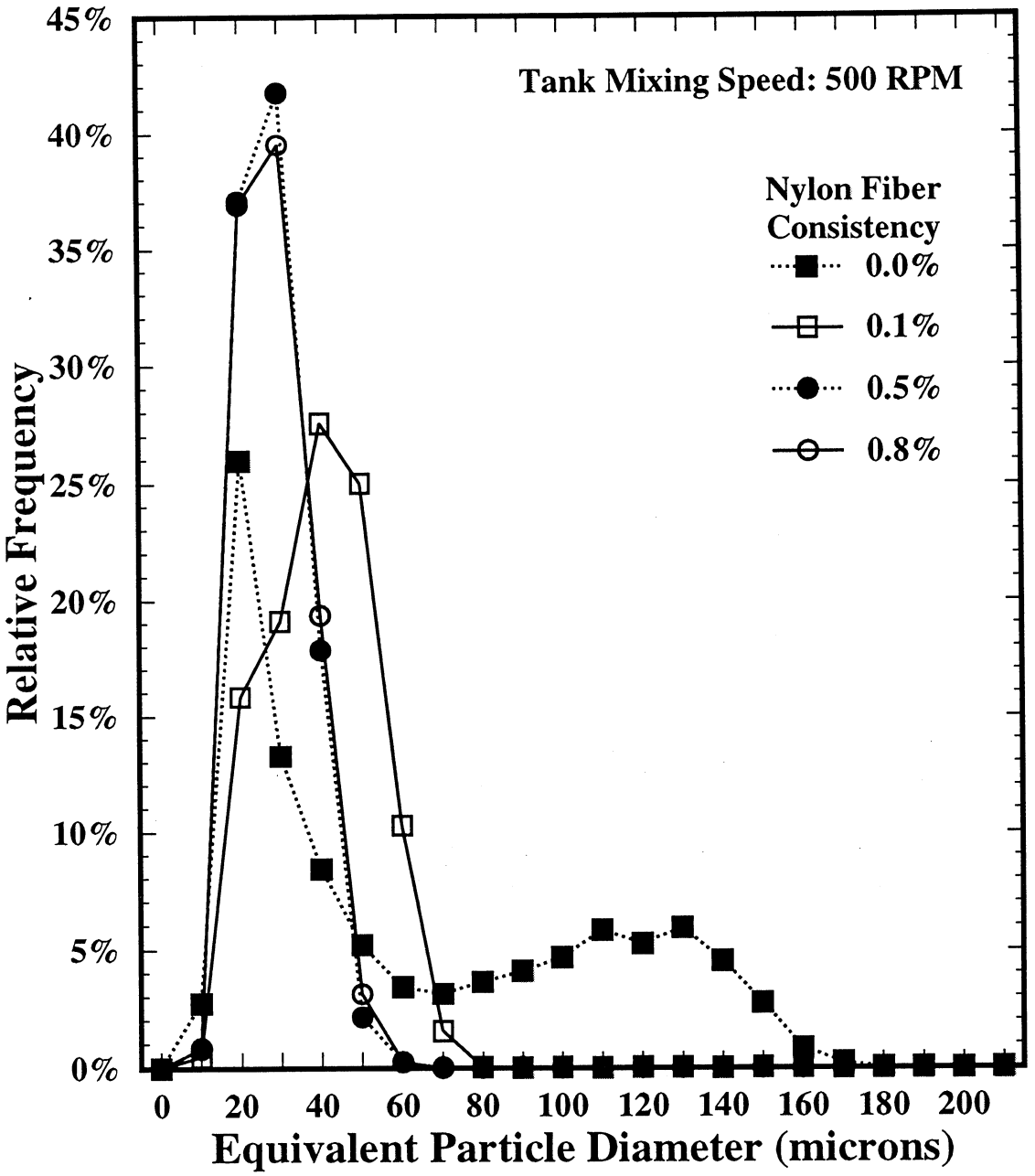

Figure 10: The effect of Nylon consistency on wax particle size distributions for a tank mixing speed of 500 RPM.

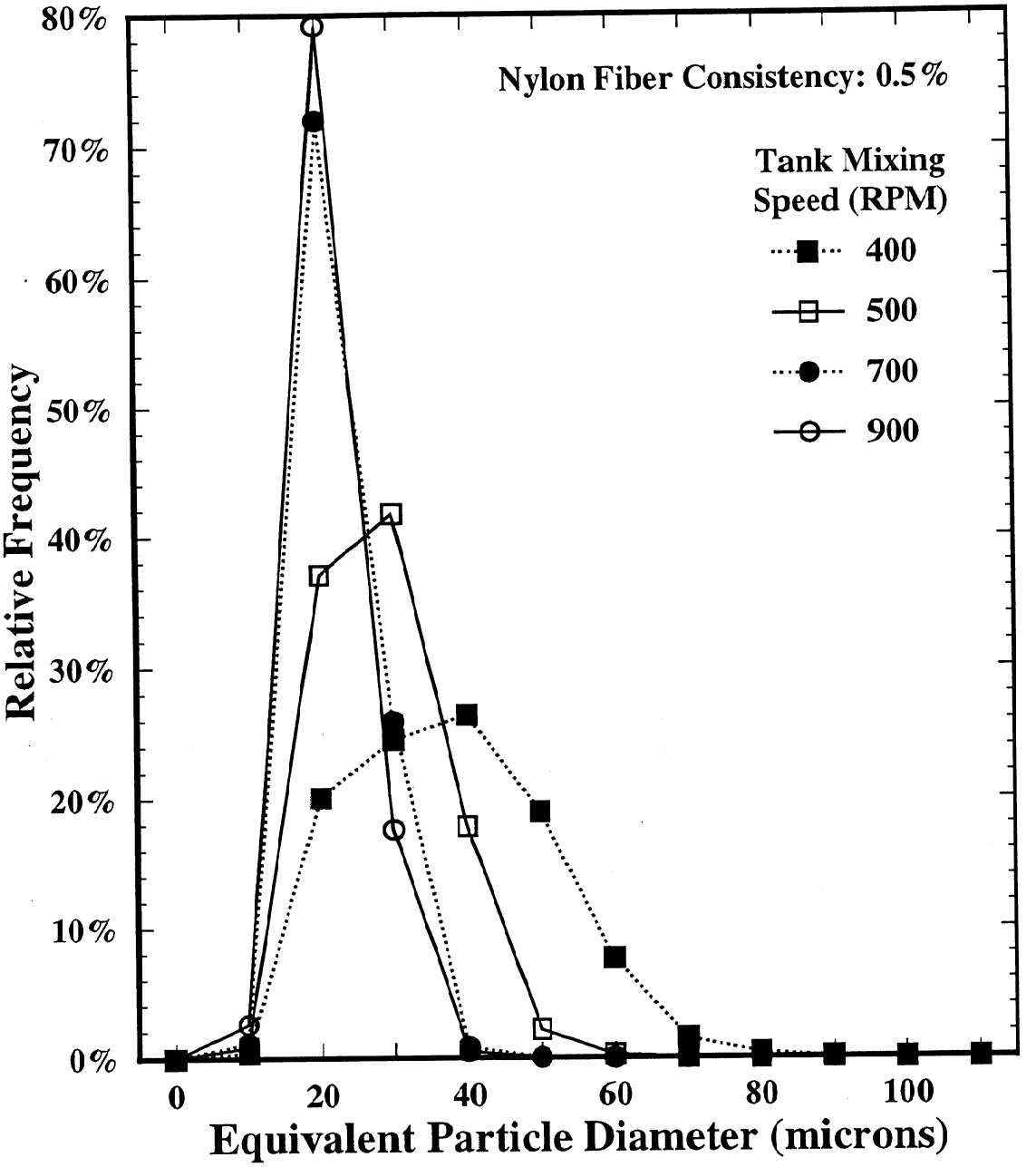

Figure 11: Effect of tank mixing speed on wax particle size distributions for a Nylon consistency of 0.5%.

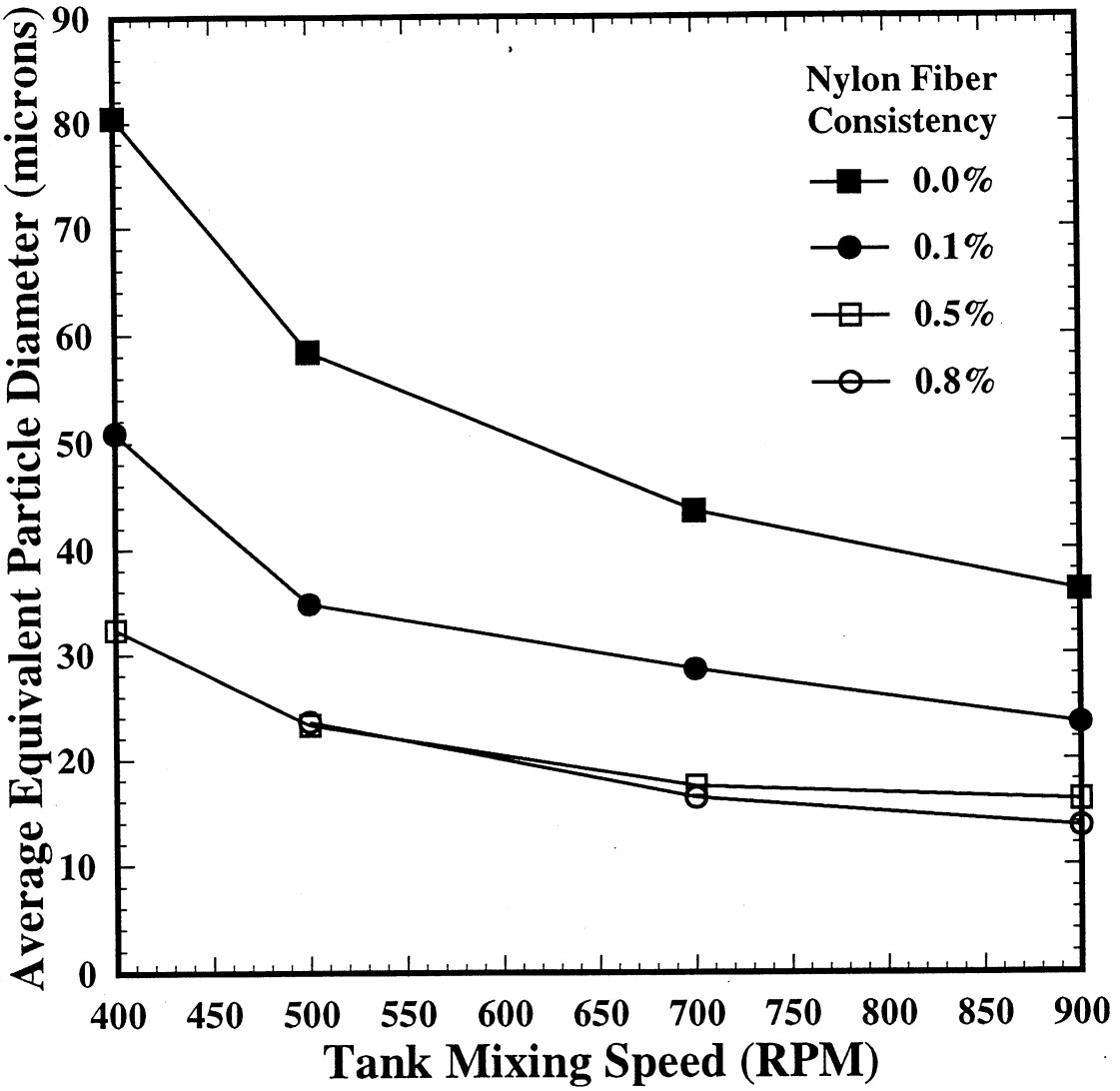

Figure 12: Average wax particle size for various Nylon fiber consistencies and tank mixing speeds.

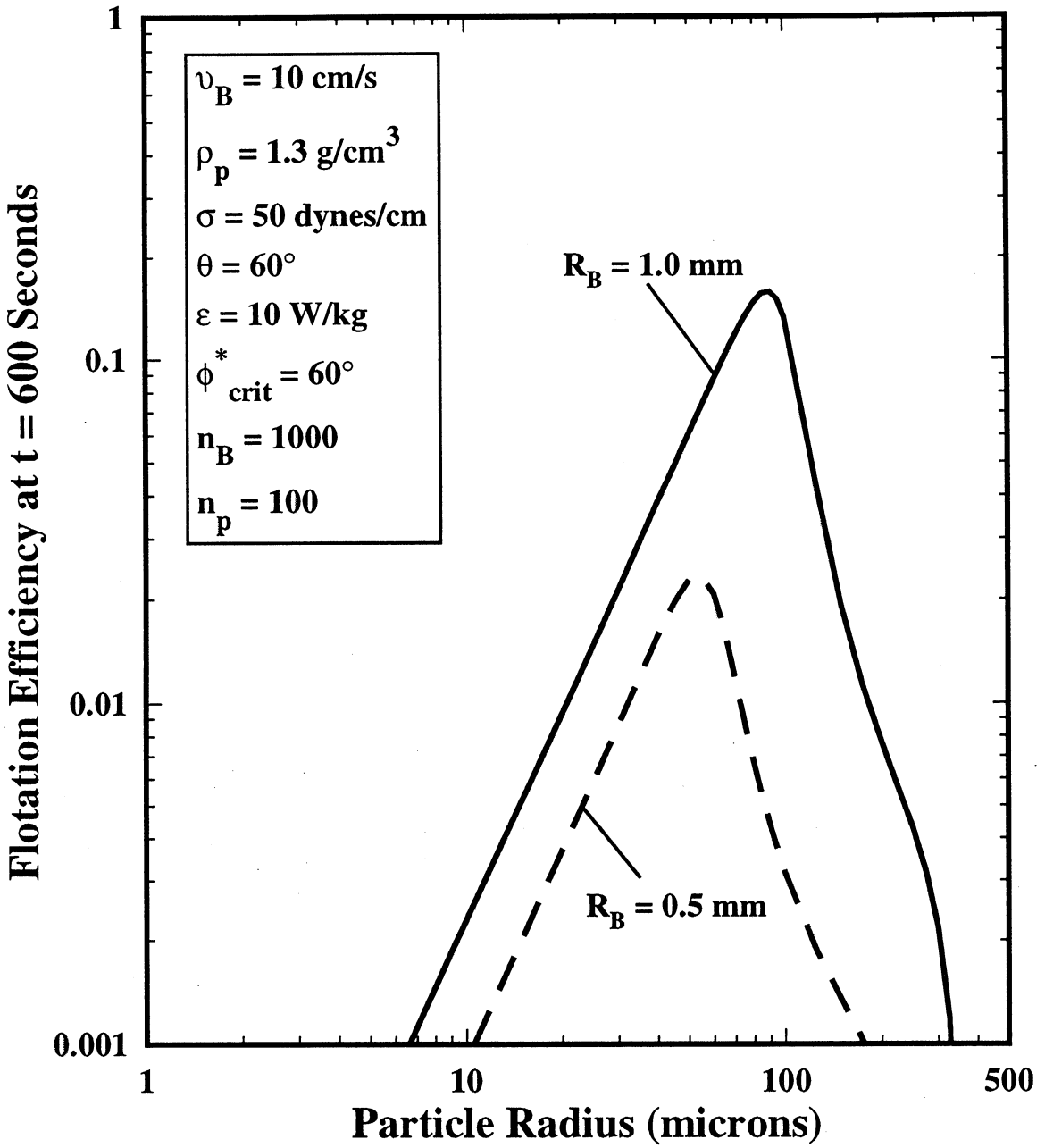

Figure 13: Flotation efficiency at t = 600 seconds as a function of particle radius, R_p, for selected bubble radii, R_B. All other parameters are fixed at the indicated conditions.